


## Article

# COCCON Measurements of XCO<sub>2</sub>, XCH<sub>4</sub> and XCO over Coal Mine Aggregation Areas in Shanxi, China, and Comparison to TROPOMI and CAMS Datasets

Qiansi Tu <sup>1,2,\*</sup> , Frank Hase <sup>3</sup>, Kai Qin <sup>4,5</sup>, Carlos Alberti <sup>3</sup>, Fan Lu <sup>4</sup>, Ze Bian <sup>4</sup>, Lixue Cao <sup>4</sup>, Jiaxin Fang <sup>1</sup>, Jiacheng Gu <sup>4</sup>, Luoyao Guan <sup>4</sup>, Yanwu Jiang <sup>1</sup>, Hanshu Kang <sup>4</sup>, Wang Liu <sup>4</sup>, Yanqiu Liu <sup>4</sup>, Lingxiao Lu <sup>4</sup>, Yanan Shan <sup>4</sup>, Yuze Si <sup>1</sup>, Qing Xu <sup>4</sup> and Chang Ye <sup>4</sup>

<sup>1</sup> School of Mechanical Engineering, Tongji University, Shanghai 201804, China; 2430516@tongji.edu.cn (J.F.); 2330400@tongji.edu.cn (Y.J.); 2430402@tongji.edu.cn (Y.S.)

<sup>2</sup> State Key Laboratory of Space Weather, Chinese Academy of Sciences, Beijing 100190, China

<sup>3</sup> Institute of Meteorology and Climate Research (IMK-ASF), Karlsruhe Institute of Technology (KIT), 76344 Eggenstein-Leopoldshafen, Germany; frank.hase@kit.edu (F.H.); carlos.alberti@kit.edu (C.A.)

<sup>4</sup> School of Environment and Spatial Informatics, China University of Mining and Technology, Xuzhou 221116, China; qinkai@cumt.edu.cn (K.Q.); luf785@cumt.edu.cn (F.L.); ts20160085p31@cumt.edu.cn (Z.B.); caolixue@cumt.edu.cn (L.C.); ts20160108p31@cumt.edu.cn (J.G.); lyguan@cumt.edu.cn (L.G.); kanghanshu@cumt.edu.cn (H.K.); ts22160040a31tm@cumt.edu.cn (W.L.); liuyanqiu@cumt.edu.cn (Y.L.); lulingxiao@cumt.edu.cn (L.L.); ts22160066a31@cumt.edu.cn (Y.S.); xuqing98@cumt.edu.cn (Q.X.); ts22160197p31@cumt.edu.cn (C.Y.)

<sup>5</sup> Shanxi Key Laboratory of Environmental Remote Sensing Applications, Xuzhou 221116, China

\* Correspondence: tuqiansi@tongji.edu.cn



**Citation:** Tu, Q.; Hase, F.; Qin, K.; Alberti, C.; Lu, F.; Bian, Z.; Cao, L.; Fang, J.; Gu, J.; Guan, L.; et al. COCCON Measurements of XCO<sub>2</sub>, XCH<sub>4</sub> and XCO over Coal Mine Aggregation Areas in Shanxi, China, and Comparison to TROPOMI and CAMS Datasets. *Remote Sens.* **2024**, *16*, 4022. <https://doi.org/10.3390/rs16214022>

Academic Editor: Stephan Havemann

Received: 3 September 2024

Revised: 15 October 2024

Accepted: 22 October 2024

Published: 29 October 2024



**Copyright:** © 2024 by the authors. Licensee MDPI, Basel, Switzerland. This article is an open access article distributed under the terms and conditions of the Creative Commons Attribution (CC BY) license (<https://creativecommons.org/licenses/by/4.0/>).

**Abstract:** This study presents the first column-averaged dry-air mole fractions of carbon dioxide (XCO<sub>2</sub>), methane (XCH<sub>4</sub>) and carbon monoxide (XCO) in the coal mine aggregation area in Shanxi, China, using two portable Fourier transform infrared spectrometers (EM27/SUNs), in the framework of the Collaborative Carbon Column Observing Network (COCCON). The measurements, collected over two months, were analyzed. Significant daily variations were observed, particularly in XCH<sub>4</sub>, which highlight the impact of coal mining emissions as a major CH<sub>4</sub> source in the region. This study also compares COCCON XCO with measurements from the Tropospheric Monitoring Instrument (TROPOMI) onboard the Sentinel-5P satellite, revealing good agreement, with a mean bias of  $7.15 \pm 9.49$  ppb. Additionally, comparisons were made between COCCON XCO<sub>2</sub> and XCH<sub>4</sub> data and analytical data from the Copernicus Atmosphere Monitoring Service (CAMS). The mean biases between COCCON and CAMS were  $-6.43 \pm 1.75$  ppm for XCO<sub>2</sub> and  $15.40 \pm 31.60$  ppb for XCH<sub>4</sub>. The findings affirm the stability and accuracy of the COCCON instruments for validating satellite observations and detecting local greenhouse gas sources. Operating COCCON spectrometers in coal mining areas offers valuable insights into emissions from these high-impact sources.

**Keywords:** greenhouse gas; XCO<sub>2</sub>; XCH<sub>4</sub>; XCO; COCCON; TROPOMI; CAMS

## 1. Introduction

Carbon dioxide (CO<sub>2</sub>) is a crucial long-lived greenhouse gas (GHG) that significantly influences the Earth's radiative energy balance and climate. According to NOAA's Global Monitoring Laboratory, the global surface CO<sub>2</sub> concentration reached approximately 419.3 parts per million (ppm) in 2023, which reflects an increase of 2.8 ppm over the past year. The primary sources of anthropogenic CO<sub>2</sub> emissions are fossil fuels and land-use changes, contributing 86% and 14% of the total emissions, respectively, over the period of 2010–2019 [1]. Methane (CH<sub>4</sub>) is another significant anthropogenic GHG, and the second-largest contributor to global warming after CO<sub>2</sub>. Despite its relatively short atmospheric lifetime of approximately 12 years, methane has a high global warming potential (GWP)

of 81.2 times that of CO<sub>2</sub> over 20 years and 27.9 times over 100 years [2]. Methane is emitted from both human activities and nature sources. About 60% of global emissions are anthropogenic, which are principally associated with fossil fuel production and use (e.g., oil and gas extraction and coal mining), waste disposal and agriculture (e.g., livestock production, rice cultivation, biomass burning) [3,4].

Carbon monoxide (CO) is a toxic and reactive gas with an atmospheric lifetime ranging from weeks to months [5]. It is generated through various processes, including the oxidation of CH<sub>4</sub>, biomass burning and the incomplete combustion of fossil fuels. In the atmosphere, CO primarily undergoes oxidation by hydroxyl radicals (OH), which acts as its primary sink and helps regulate its concentration [6]. An increase in CO levels reduces the availability of OH, which in turn influences the lifetime of CH<sub>4</sub>. Consequently, CO emissions are known to contribute to increased radiative forcing, classifying CO as an indirect GHG [7]. Additionally, CO is involved in the formation of ground-level ozone (O<sub>3</sub>), a harmful air pollutant that can exacerbate respiratory conditions. Understanding and precisely monitoring CO<sub>2</sub>, CH<sub>4</sub> and CO gases are essential for identifying their sources, sinks and trends. Comprehensive information of the spatiotemporal distributions of these gases provides a fundamental basis for accurately identifying emissions and sources, and for evaluating their environmental and regulatory impacts [8,9].

For many decades, atmospheric measurements of CO<sub>2</sub>, CH<sub>4</sub> and CO have been conducted using in situ surface-based networks and occasional aircraft campaigns [10–14]. However, these methods have been limited to a few locations and have sampled the atmosphere non-uniformly. Recent advancements in remote sensing technologies, both space-based and ground-based, have significantly enhanced our ability to detect and monitor these gases globally. Satellites, such as the Sentinel-5 Precursor (S5P), offer extensive global coverage, allowing for detailed trend analysis and the refinement of emission inventories, not only at a global scale, but also at regional and local scales [9,15–19].

Ground-based column abundance measurements using solar-viewing near-infrared spectrometers are comprehensively employed to validate satellite observations, ensuring the accuracy and reliability of the data [9,20,21]. The Total Carbon Column Observing Network (TCCON) is a global network of ground-based Fourier transform infrared (FTIR) spectrometers, providing highly precise column-averaged dry-air mole fractions of the gas (X<sub>gas</sub>) values for CO<sub>2</sub> (XCO<sub>2</sub>), CH<sub>4</sub> (XCH<sub>4</sub>) and CO (XCO), amongst other gases [22]. X<sub>gas</sub> is defined by the following equation:

$$X_{\text{gas}} = 0.2095 \times \frac{\text{column}_{\text{gas,dry}}}{\text{Column}_{\text{O}_2,\text{dry}}},$$

where 0.2095 is the dry-air O<sub>2</sub> mole fraction.

Recently, the Collaborative Carbon Column Observing Network (COCCON) has emerged, using a portable, low-resolution FTIR spectrometer (Bruker EM27/SUN) as its standard instrument, serving as a valuable complement to the TCCON network [23–26]. These portable COCCON instruments are characterized by stability and the ability to retrieve GHGs concentrations with high precision and accuracy. As a result, they are well-suited for deployment in diverse environments, including high-latitude regions, deserts and urban areas [21,27–36].

Alongside the increasing development of GHG sensors, both in orbit and through ground-based remote sensing networks, the Copernicus Atmosphere Monitoring Service (CAMS) is a service implemented by the European Centre for Medium-Range Weather Forecasts (ECMWF) on behalf of the European Commission, using the Numerical Weather Prediction (NWP) Integrated Forecasting system for Composition (C-IFS) to deliver consistent and high-quality data related to air pollution and atmospheric composition, such as greenhouse gases, on a global scale [37,38].

This study presents the first COCCON observations conducted in Shanxi, China, focusing on the XCO<sub>2</sub>, XCH<sub>4</sub> and XCO measured over Zhangzi County. It includes a comparison between the COCCON XCO data and the XCO measurements from the TROPOspheric

Monitoring Instrument (TROPOMI), on board the S5P satellite. Additionally, this study analyzes the collocated  $\text{XCO}_2$  and  $\text{XCH}_4$  from COCCON in comparison with the analysis datasets from CAMS.

## 2. Materials and Methods

### 2.1. Sites Description

Shanxi is situated in northern China, and it is characterized by mountainous terrain. In 2023, Shanxi, one of the China's leading coal-producing provinces, produced approximately 1.37 billion tons of coal, accounting for about 30% of the country's total coal production. Zhangzi County is situated in the southeastern part of Shanxi and on the southwestern edge of the Shangdang Basin. It lies in the transitional zone between the Taiyue Mountains and the Taihang Mountains. Surrounded by mountains on three sides and bordered by a vast plain on the remaining side, the county has a significant portion of its land dedicated to agriculture, with cultivated areas comprising of approximately 40% of its total land area. Zhangzi County has proven coal reserves amounting to 5.97 billion tons. These mines are part of the Qinshui coal field. Currently, there are 10 large-scale coal mines operating in the county, which collectively produced 34 million tons of raw coal in 2022 (<http://www.zhangzi.gov.cn/zzxxgk/zfxxgk/zfxxgkml/sjhd/202305/P020230525391512084152.pdf>, last access: 21 August 2024). Among them, a local coal mine (close to site10, Figure 1) is notable for its annual production exceeding 7 million tons.

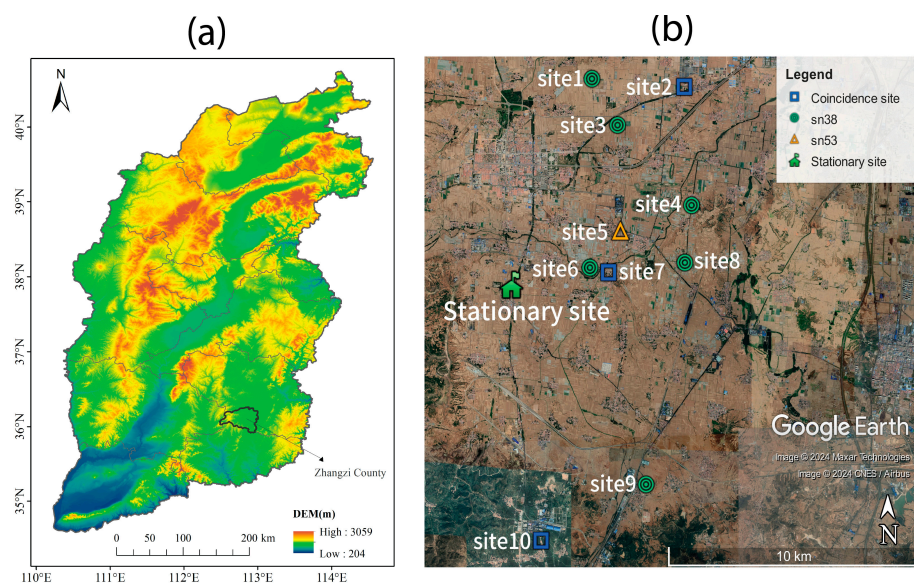


**Figure 1.** (a) A terrain map showing Shanxi Province and the location of Zhangzi County. (b) A map showing the locations of two COCCON spectrometers in Zhangzi County, within Shanxi province. The SN53 instrument was primarily positioned at the stationary site. Green circles indicate locations where the SN38 instrument was deployed, while orange triangles represent sites for the SN53 instrument. Blue rectangles denote locations where both instruments were used on different days. The base map is sourced from © Google Earth, Image © 2024 Maxar Technologies; Image © 2024 CNES/Airbus.

### 2.2. COCCON

The emergence of portable, low-resolution and solar-viewing FTIR instruments, such as EM27/SUN, has significantly enhanced global coverage of GHG observations [25]. The EM27/SUN is a compact and mobile instrument that was developed by the Karlsruhe Institute of Technology (KIT) in collaboration with Bruker Optics GmbH, Ettlingen, Germany [25,26]. The spectrometer records double-sided DC coupled interferograms in the NIR window using two indium gallium arsenide (InGaAs) detectors at room temperature. It has a spectral resolution of  $0.5 \text{ cm}^{-1}$ , which, with careful calibration, provides precision



and accuracy comparable to that of TCCON [39]. The interferograms are processed using a preprocessing tool and the PROFFAST nonlinear least squares fitting algorithm, the code development being supported by the ESA in the framework of COCCON-PROCEEDS projects. The PROFFAST retrieval algorithm scales a priori profiles to retrieve the total column of trace gases, including  $\text{CO}_2$ ,  $\text{CH}_4$  and  $\text{CO}$ .

More than 200 EM27/SUN instruments are currently operated worldwide by various research groups. Studies have demonstrated that the instrument is appropriate for both field campaigns and long-term deployment at fixed sites, offering the ability to complement TCCON by extending observational coverage and enhancing data collection in various locations [31,33,34,40–43]. In this context, the Collaborative Carbon Column Observing Network (COCCON) was established to further advance and integrate these observational efforts. COCCON also implemented as international travel standard spectrometers unit for evaluating the consistency of GHG measurements across different TCCON stations [24].

Two COCCON instruments were used to assess columnar greenhouse gas abundances, focusing on coal mine aggregation areas between July and September 2022. This collaborative project involved Tongji University and China University of Mining and Technology (CUMT), as well as the Karlsruhe Institute of Technology (KIT), Germany. The instruments were first shipped from Karlsruhe, Germany, to Xuzhou, China. Upon arrival in Xuzhou, side-by-side measurements were conducted at the CUMT campus ( $34.22^\circ\text{N}$ ,  $117.19^\circ\text{E}$ ) in Xuzhou to ensure that the instruments were functioning properly and undamaged after their long-distance transport (Figure 2). Following this, the instruments were transported to Zhangzi County (back to Xuzhou), where similar calibration measurements were performed before (and after) the field campaign. These calibrations were crucial for ensuring the accuracy of the observations, despite initial calibrations having been completed with a reference COCCON instrument at Karlsruhe Institute of Technology (KIT).



**Figure 2.** Side-by-side calibration measurements were performed at CUMT Campus in Xuzhou prior to shipment to Shanxi province. Simultaneous solar observations from two COCCON instrument were analyzed to verify the temporal invariability of instrumental characteristics and to derive intercalibration factors for  $\text{XCO}_2$ ,  $\text{XCH}_4$  and  $\text{XCO}$ .

During the campaign, one COCCON instrument (SN53) was mostly positioned at a stationary site (see Figure 1) for the entire study period, except for 19 August (site5), 23 August (site2) and 30 August–1 September (site7). The second COCCON instrument (SN38) was moved to different locations daily, depending on the prevailing wind direction, to capture downwind signals with respect to the SN53 instrument. Observed interferograms were processed with PROFFAST v2.4 retrieval algorithms to obtain trace gases abundances.

In addition to the abundances of the target gases, PROFFAST also provides a sensitive indication (XAIR) for the detection of instrumental drifts and operation problems [24,39]. XAIR quantity is calculated from observed columns of O<sub>2</sub> and H<sub>2</sub>O, and from ground pressure:

$$\text{Xair} = \frac{0.2095}{\text{Column}_{\text{O}_2} \cdot \bar{\mu}} \left( \frac{P_s}{g} - \text{column}_{\text{H}_2\text{O}} \cdot \mu_{\text{H}_2\text{O}} \right), \quad (1)$$

where  $\bar{\mu}$  and  $\mu_{\text{H}_2\text{O}}$  represent the molecular mass for dry air mass and water vapor, respectively. TCCON also uses XAIR as a supplementary method to check for consistency. Note that XAIR values calculated by PROFFAST are inverted compared to values by the GGG algorithm in TCCON.

### 2.3. TROPOMI XCO Products

The S5P satellite, launched in October 2017, is an Earth observation satellite developed by European Space Agency as part of the Copernicus Programme. It was designed to maintain continuity of atmospheric observations between the Envisat and Sentinel-5 missions. S5P provides comprehensive data on various trace gases and aerosol properties with global coverage on a daily basis and an overpass time of 13:30 local solar time [19]. The payload of the mission is the TROPOMI, a nadir-viewing imaging spectrometer that employs passive remote-sensing techniques. TROPOMI measures backscattered solar radiation across multiple spectral bands, including ultraviolet (UV), visible (VIS), near-infrared (NIR) and short-wave infrared (SWIR), for monitoring atmospheric composition and detecting environmental changes [18,19]. The instrument operates in a push-broom configuration with a broad swatch of approximately 2600 km and an unprecedented spatial resolution of  $5.5 \times 7 \text{ km}^2$  ( $7 \times 7 \text{ km}^2$  prior to August 2019) [9].

Total column abundances of CO are retrieved from the TROPOMI SWIR module at  $2.3 \text{ }\mu\text{m}$  using the SICOR physics-based retrieval algorithm (<https://sentinel.esa.int/documents/247904/2476257/Sentinel-5P-TROPOMI-ATBD-Carbon-Monoxide-Total-Column-Retrieval.pdf>, last access: 28 August 2024) [44]. Ref. [45] compared the TROPOMI XCO with a large number of TCCON FTIR stations, presenting a relative mean bias of  $9.22 \pm 3.45\%$  for the standard TCCON XCO. In this study, the TROPOMI XCO L2 data during the study period are investigated. To ensure the satellite products are recorded under clear-sky and low-cloud atmospheric conditions, a quality value ( $qa \geq 0.7$ ) is applied.

### 2.4. CAMS XCO<sub>2</sub> and XCH<sub>4</sub> Products

CAMS provides a range of products, including global near-real-time analysis, reanalysis and forecast of the GHGs for recent years [46–49]. In this work, the CAMS XCH<sub>4</sub> and XCO<sub>2</sub> analysis dataset has a spatial resolution of  $29 \text{ km}$  ( $0.25^\circ \times 0.25^\circ$ ) and a temporal resolution of 6 h.

## 3. Results and Discussion

### 3.1. Side-by-Side Measurements

Instrument calibration is crucial for ensuring accuracy when multiple instruments are used in a field campaign. The COCCON instruments were checked and calibrated with respect to a common reference unit (the EM27/SUN spectrometer SN37) at KIT before delivery to the end users. However, instruments can experience unexpected mechanical shocks, such as impacts or vibrations, particularly during transportation [23]. Therefore, solar side-by-side calibration measurements are necessary both before and after the campaign to verify the temporal invariability of instrumental characteristics and to derive intercalibration factors for retrievals [40].

The initial calibration took place from 21 July to 24 July, after the instruments were shipped from Karlsruhe, Germany to Xuzhou, China. After transporting the instruments to Zhangzi, a 2-day measurement period was conducted. Additional calibration measurements were performed during 21–23 September, after the instruments were shipped back to Xuzhou.

To determine the calibration factors, measurements were collected on clear-sky days with empirical instrument-specific solar zenith angles of less than 50 degrees for each target gas. To minimize the impact of scattered clouds during the measurements, a strict filtering process was applied, excluding observations in which the difference between individual XAIR values and the mean value exceeded 0.001.

The calibration process involved scaling the retrievals ( $X_{CO_2}$ ,  $X_{CH_4}$  and  $X_{CO}$ ) from the SN38 instrument to align with those from the SN53 instrument, as follows:

$$X_{gasSN38}^{cali} = X_{gasSN38}^{unc} \times f_{gas}$$

where  $X_{gasSN38}^{cali}$  represents the calibrated retrieval for the SN38 instrument, while  $X_{gasSN38}^{unc}$  denotes the uncalibrated retrieval.  $f_{gas}$  indicates the slope of the fitting line established from the side-by-side measurements of the SN38 and SN53 instruments. Note that the fitting line was constrained to pass through the origin, resulting in slopes of 1.0027 for  $X_{CO_2}$ , 0.9978 for  $X_{CH_4}$  and 0.9810 for  $X_{CO}$ .

Figure 3 illustrates the 5-min average time series of the uncalibrated COCCON measurements taken during the campaign in Zhangzi County and after the campaign in Xuzhou. The time series from both periods exhibit generally similar trends. However, on 2 August, around noon, outliers in  $X_{CO}$  were observed due to cloud cover, which were not filtered out during the data processing. This issue did not affect the  $X_{CO_2}$  and  $X_{CH_4}$  measurements on this day because the  $CO_2$ ,  $CH_4$  and  $O_2$  columns were retrieved from the same primary channel, whereas the  $CO$  columns were obtained from the secondary channel. Different kinds of disturbances in the measured  $CO_2$ ,  $CH_4$  and  $O_2$  columns are compensating when calculating  $X_{CO_2}$  and  $X_{CH_4}$  by rationing the target gas column over the co-observed  $O_2$  columns.

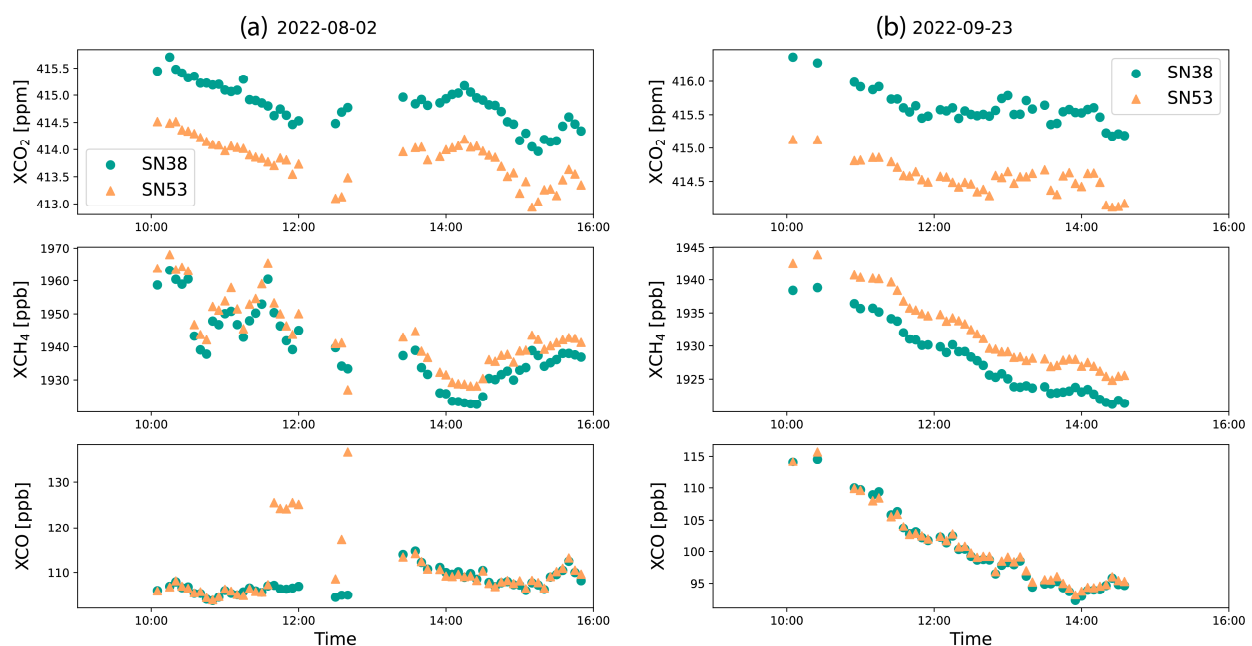


**Figure 3.** Side-by-side uncalibrated measurements from two example days (a) during (Zhangzi, 2022-08-02) and (b) after (Xuzhou, 2022-09-03) the campaign.

Figure 4 presents the correlations of the calibrated retrievals from SN38 instrument with respect to those from SN53 instrument. Different colors in the figure represent measurements taken on different days. The mean biases observed are as follows:  $-0.0002 \pm 0.4143$  ppm for  $X_{CO_2}$ ,  $-0.0054 \pm 1.7717$  ppb for  $X_{CH_4}$  and  $0.2225 \pm 4.9755$  ppb for  $X_{CO}$ . Notably, some data outliers, especially on 24–25 July and 2 August, are mainly due to cloud cover during the measurements. The variation in solar intensity due to

cloud disturbances did not exceed the filtering criteria and therefore the trace gas results were not excluded during the data processing.

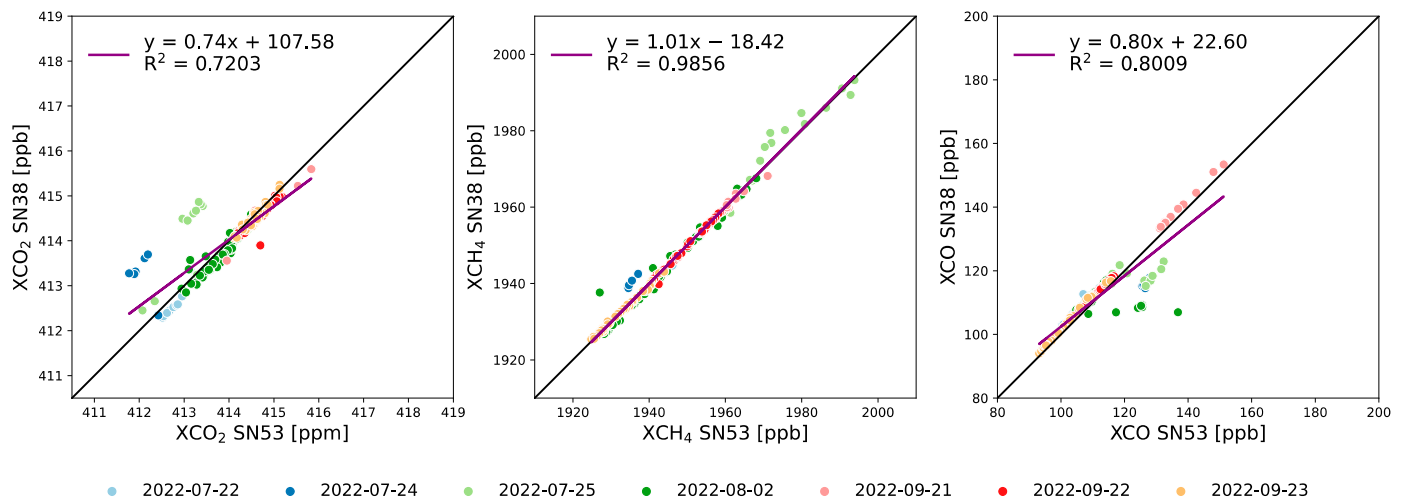


**Figure 4.** Correlations of calibrated XCO<sub>2</sub>, XCH<sub>4</sub> and XCO between the two instruments.

Note that the following XCO<sub>2</sub>, XCH<sub>4</sub> and XCO results refer to the value obtained after applying the instrument-specific calibration factors.

### 3.2. COCCON Observations

#### 3.2.1. XAIR

Figure 5 presents the time-series of XAIR for two instruments from August to September. The performance indicator parameter, XAIR, showed generally consistent values around 1 for both instruments, with specific values of  $1.004 \pm 0.0011$  for SN38 and  $0.9975 \pm 0.0009$  for SN53 (Table 1), indicating no obvious instrumental drifts or operation problems during the period. It also further demonstrated that the COCCON instrument is robust for long-distance transport and field campaigns.

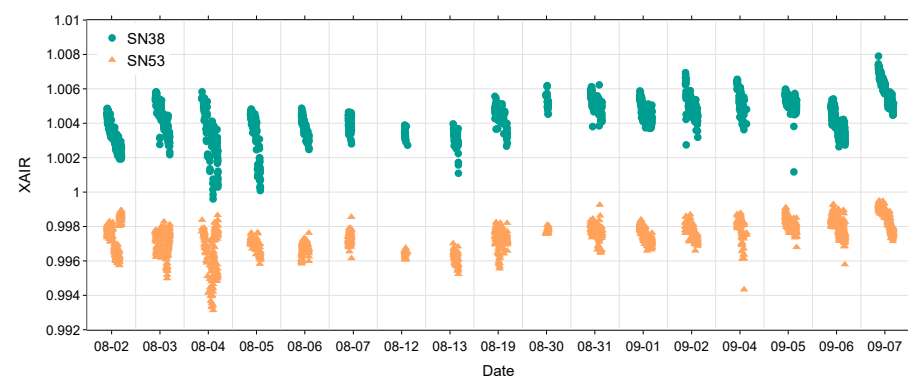


**Figure 5.** Time series of XAIR during field campaign in Zhangzi County. XAIR is a sensitive indication for instrumental drifts and operation problems.

**Table 1.** Summary of COCCON XCO<sub>2</sub>, XCH<sub>4</sub> and XCO measurements observed in Zhangzi County.

| COCCON | XAIR                | XCO <sub>2</sub> (ppm) | XCH <sub>4</sub> (ppb) | XCO (ppb)          |
|--------|---------------------|------------------------|------------------------|--------------------|
| SN38   | $1.004 \pm 0.0011$  | $413.66 \pm 1.20$      | $1999.71 \pm 73.69$    | $123.92 \pm 19.13$ |
| SN53   | $0.9975 \pm 0.0009$ | $413.64 \pm 1.08$      | $2004.10 \pm 85.62$    | $123.96 \pm 19.15$ |

### 3.2.2. XCO<sub>2</sub>

Although the two instruments were positioned up to approximately 10 km apart, their observations generally exhibited similar trends in XCO<sub>2</sub> level (Figure 6). The mean XCO<sub>2</sub> values were  $413.66 \pm 1.20$  ppm for SN38 and  $413.64 \pm 1.08$  ppm for SN53, respectively. The averaged bias between the instruments over the field campaign was  $0.02 \pm 0.89$  ppm. The maximal difference up to 5.09 ppm occurred on the morning of 7 September, when SN38 was positioned in the northeast (site2) and SN53 at the stationary site. The significant increase in XCO<sub>2</sub> may be attributed to the proximity of SN38 to a power plant, which is a different source compared to the observations from SN53.

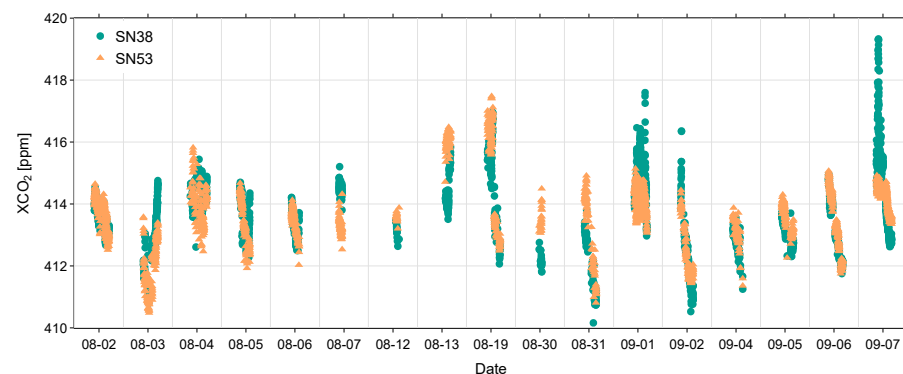


**Figure 6.** Similar to Figure 5, but for XCO<sub>2</sub>.

### 3.2.3. XCH<sub>4</sub>

XCH<sub>4</sub> exhibits higher variability compared to XCO<sub>2</sub>, reflecting the influence of local coal mines, which are major sources of CH<sub>4</sub> emissions in this region [50]. Over the measurement period, the two instruments recorded similar mean values:  $1999.71 \pm 73.69$  ppb for SN38 and  $2004.10 \pm 85.62$  ppb for SN53 (see Figure 7). The XCH<sub>4</sub> levels and their variation in this coal mine aggregation area were generally higher compared to urban areas, such as Xuzhou, where the mean values were  $1942.67 \pm 13.02$  ppb for SN38 and  $1942.15 \pm 11.57$  ppb for SN53.

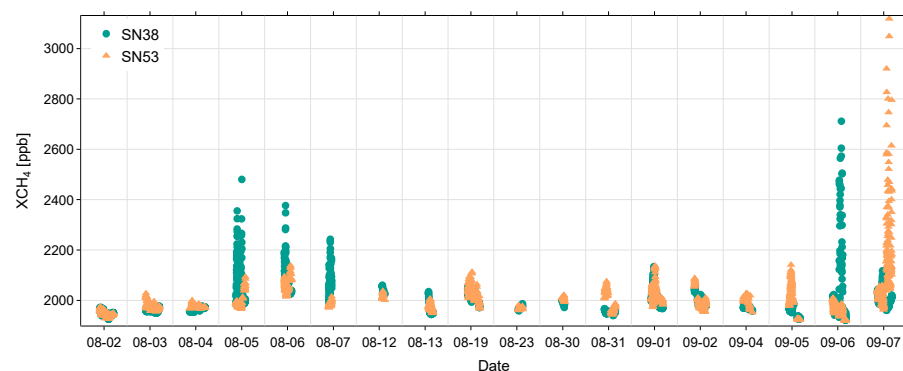


**Figure 7.** Similar to Figure 5, but for XCH<sub>4</sub>.

The average bias between the instruments was  $-4.39 \pm 107.68$  ppb during the field campaign, corresponding to a small relative difference of approximately  $-0.22\%$ . However, individual differences varied significantly, ranging between  $-1138.89$  ( $-57\%$ ) on 7 September and  $748.19$  ppb ( $37\%$ ) on 6 September. Significant XCH<sub>4</sub> enhancements were observed when the instruments were positioned at site10, close to the local coal mine in the south, i.e., on 5–7 August and 6 September (after 1 pm) for SN38 and on 7 September (after 1 pm) for SN53.



Figure 8 shows an example day, when SN53 was relocated from its stationary site to site10 after 1 pm. This move resulted in a significant increase in  $\text{XCH}_4$  levels, with an average value of  $2128.34 \text{ ppb} \pm 183.94 \text{ ppb}$ , ranging from 1963.10 to 3118.71 ppb.

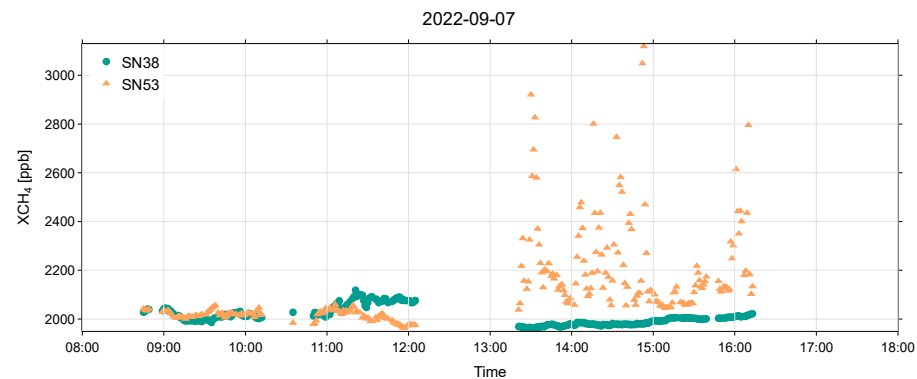


**Figure 8.** Time series of  $\text{XCH}_4$  for the example day of 7 September.

### 3.2.4. XCO

The averaged XCO levels in the coal mining areas are  $123.92 \pm 19.13 \text{ ppb}$  for SN38 and  $123.96 \pm 19.15 \text{ ppb}$  for SN53 (Figure 9). In comparison, the XCO levels in urban areas like Xuzhou are slightly lower, with averages of  $113.86 \pm 12.06 \text{ ppb}$  for SN38 and  $111.98 \pm 11.83 \text{ ppb}$  for SN53. This results in a mean difference of approximately 10 ppb in this region. The elevated XCO concentrations in the mining areas are mostly attributed to the incomplete combustion of  $\text{CH}_4$  emitted from coal mining activities or the natural gas used in residential areas [51–53].

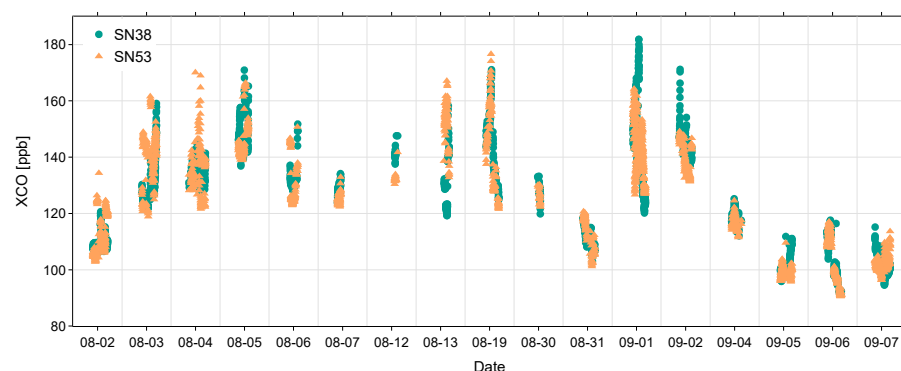


**Figure 9.** Similar to Figure 5, but for XCO.

### 3.3. Comparison Between COCCON and TROPOMI Datasets

Figure 10 presents the correlation in XCO between TROPOMI and COCCON. The COCCON XCO values were collocated with TROPOMI XCO within 2 h of the satellite overpass over Zhangzi. The spatial collocation criterion was set to a 20 km radius for TROPOMI data. Additionally, satellite measurements were restricted to those with a quality assurance value (qa) equal to or larger than 0.7, representing measurements under clear-sky conditions or the presence of low-level clouds.

The correlation between COCCON and TROPOMI XCO shows good agreement, with an  $R^2$  value of 0.7042 and a mean difference of  $7.15 \pm 9.49 \text{ ppb}$  for both instrument measurements. When collocated TROPOMI XCO points were collected within larger spatial radii of 50 km (see Appendix A Figure A1), the resulting bias increased to  $8.74 \pm 10.29 \text{ ppb}$ . The statistics are summarized in Table 2.

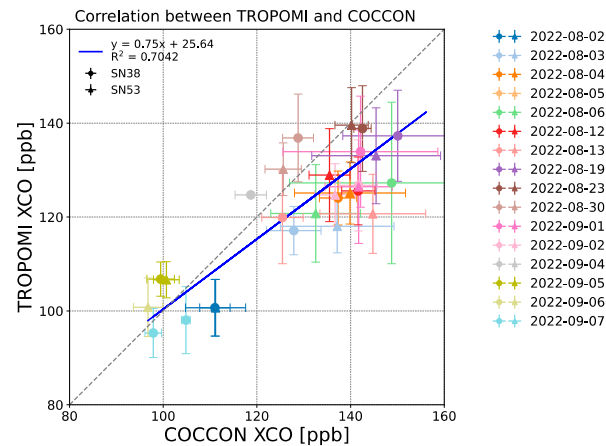


**Figure 10.** Correlation plot between TROPOMI and COCCON XCO measurements. Circle and triangle symbols represent collocated SN38 and SN53 data, respectively. Error bar denotes the standard deviations. Different colors denote measurements on different days.

**Table 2.** The mean biases in XCO measurements between COCCON and TROPOMI, as well as in XCO<sub>2</sub> and XCH<sub>4</sub> measurements between COCCON and CAMS.

|                |      | XCO <sub>2</sub> (ppm) | XCH <sub>4</sub> (ppb) | XCO (ppb)   |
|----------------|------|------------------------|------------------------|-------------|
| COCCON-TROPOMI | SN38 | --                     | --                     | 5.91 ± 9.60 |
|                | SN53 | --                     | --                     | 8.67 ± 9.51 |
| COCCON-CAMS    | SN38 | −6.43 ± 1.73           | 14.05 ± 34.75          | --          |
|                | SN53 | −6.42 ± 1.81           | 16.93 ± 28.71          | --          |

### 3.4. Comparison Between COCCON and CAMS Datasets

Figures 11 and 12 present correlations between the collocated CAMS and COCCON XCO<sub>2</sub> and XCH<sub>4</sub> for SN38 and SN53, respectively. The COCCON measurements were averaged from data collected 2 h before and after 2 p.m., local time, with error bars representing standard deviations. The CAMS results were obtained from the mean value within a 20 km radius at 2 p.m., local time.

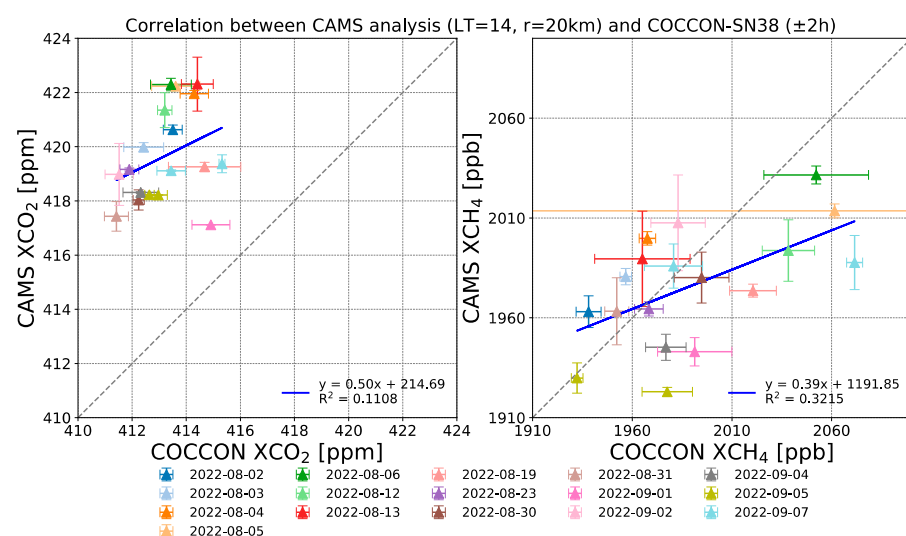


**Figure 11.** Correlation plot between CAMS and COCCON SN53 for XCO<sub>2</sub> and XCH<sub>4</sub>.

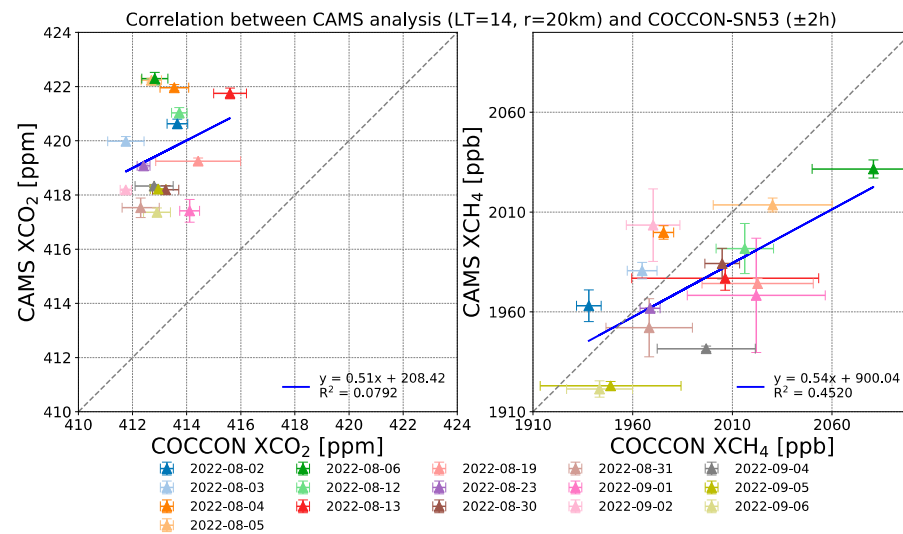


Figure 12. Similar to Figure 11 but for COCCON SN38.

The collocated CAMS data generally show higher XCO<sub>2</sub> and lower XCH<sub>4</sub> compared to the COCCON results. The CAMS modeled values that were  $6.43 \pm 1.73$  ppm higher in XCO<sub>2</sub> and  $14.05 \pm 34.75$  ppb lower in XCH<sub>4</sub> compared to SN38 and  $6.42 \pm 1.81$  and  $16.93 \pm 28.71$  ppb compared to SN53. For some days, such as on 5 August (13 August), SN38 (SN53) measured significant XCH<sub>4</sub> signals around 2 p.m., local time, resulting in a high standard deviation (error bar).

#### 4. Conclusions

In this paper, total columns of CO<sub>2</sub>, CH<sub>4</sub> and CO were measured for the first time in Zhangzi County, a coal mine aggregation area in China. Two portable solar-viewing FTIR instruments (SN38 and SN53) within the framework of the COCCON network were employed over two months, August and September, 2022.

Side-by-side measurements were conducted after the instruments were shipped to China, during the campaign and after the campaign, presenting good consistence between the two instruments. The calibrated results indicated minimal biases in two instruments. Additionally, the performance indicator parameter, XAIR, during the observation period showed minor variations (standard deviation < 0.21%). These results further highlight the robust performance of the COCCON instruments.

Both COCCON instruments observed similar mean values for XCO<sub>2</sub>, XCH<sub>4</sub> and XCO, although there were large differences on various days. Among these gases, XCH<sub>4</sub> exhibited the highest variability for both instruments, reflecting the influence of coal mine emissions, a major source of CH<sub>4</sub> in this region.

The COCCON results were also compared with TROPOMI (for XCO) and CAMS analysis (for XCO<sub>2</sub> and XCH<sub>4</sub>) datasets, showing generally better agreements in COCCON–TROPOMI than COCCON–CAMS. TROPOMI observed higher values of  $5.91 \pm 9.60$  ppb and  $8.67 \pm 9.51$  ppb in XCO for SN38 and SN53, respectively. CAMS generally overestimated XCO<sub>2</sub>, reporting values of  $6.43 \pm 1.73$  ppm for SN38 and  $6.42 \pm 1.81$  ppm for SN53. In contrast, CAMS underestimated XCH<sub>4</sub>, with values of  $14.05 \pm 34.7$  ppb and  $16.93 \pm 28.71$  ppb compared to COCCON for SN38 and SN53, respectively.

The stability and accuracy of COCCON ensure its capability for validating satellite observations and detecting local GHG sources. The operation of the COCCON spectrometer in coal mine areas will provide critical insights into emissions from such high-impact sources. Combined with modeling efforts, COCCON measurements will enhance the accuracy of emission source estimations.

**Author Contributions:** Conceptualization, Q.T., F.H. and K.Q.; Data curation, Q.T.; Formal analysis, Q.T.; Funding acquisition, Q.T. and K.Q.; Investigation, Q.T., F.L., Z.B., L.C., J.F., J.G., L.G., Y.J., H.K., W.L., Y.L., L.L., Y.S. (Yanan Shan), Q.X. and C.Y.; Methodology, Q.T.; Project administration, Q.T., F.H. and K.Q.; Resources, F.H. and C.A.; Visualization, Q.T. and Y.S. (Yuze Si); Writing—original draft, Q.T.; Writing—review and editing, F.L. All authors have read and agreed to the published version of the manuscript.

**Funding:** This research was funded by the National Natural Science Foundation of China (grant no. 42305138), the Specialized Research Fund for State Key Laboratories, the People’s Government of Shanxi Province (grant no. 202101090301013), and the Fundamental Research Funds for the Central Universities.

**Data Availability Statement:** The EM27/SUN FTIR spectrometer data over Zhangzi, China, are available upon request. The TROPOMI observations are publicly available from the Copernicus Open Access Hub (<https://scihub.copernicus.eu/>, ESA, 2021, accessed on 22 August 2024).

**Acknowledgments:** We would like to thank Copernicus User Support Team at ECMWF for providing the CAMS model data. We thank the TROPOMI team for making CH<sub>4</sub> and CO data publicly available.

**Conflicts of Interest:** The authors declare no conflicts of interest.

## Appendix A

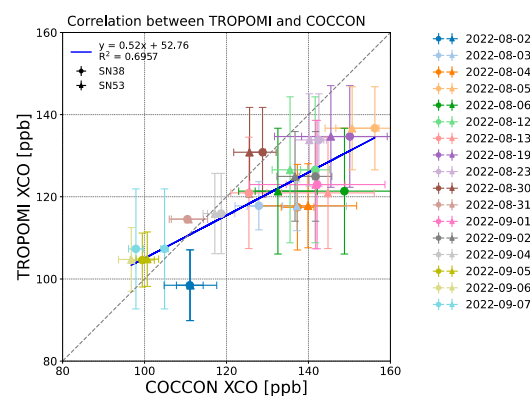


**Figure A1.** Similar to Figure 10 but with a spatial criterion of 50 km radius for collocated TROPOMI XCO.

## References

1. Friedlingstein, P.; O’Sullivan, M.; Jones, M.W.; Andrew, R.M.; Hauck, J.; Olsen, A.; Peters, G.P.; Peters, W.; Pongratz, J.; Sitch, S.; et al. Global Carbon Budget 2020. *Earth Syst. Sci. Data* **2020**, *12*, 3269–3340. [CrossRef]
2. Intergovernmental Panel On Climate Change (Ipcc) (Ed.) *Climate Change 2022—Mitigation of Climate Change: Working Group III Contribution to the Sixth Assessment Report of the Intergovernmental Panel on Climate Change*, 1st ed.; Cambridge University Press: Cambridge, UK, 2023; ISBN 978-1-00-915792-6.
3. Saunio, M.; Stavert, A.R.; Poulter, B.; Bousquet, P.; Canadell, J.G.; Jackson, R.B.; Raymond, P.A.; Dlugokencky, E.J.; Houweling, S.; Patra, P.K.; et al. The Global Methane Budget 2000–2017. *Earth Syst. Sci. Data* **2020**, *12*, 1561–1623. [CrossRef]
4. Maasakkers, J.D.; Varon, D.J.; Elfarsdóttir, A.; McKeever, J.; Jervis, D.; Mahapatra, G.; Pandey, S.; Lorente, A.; Borsdorff, T.; Foorthuis, L.R.; et al. Using Satellites to Uncover Large Methane Emissions from Landfills. *Sci. Adv.* **2022**, *8*, eabn9683. [CrossRef] [PubMed]
5. Novelli, P.C.; Masarie, K.A.; Lang, P.M. Distributions and Recent Changes of Carbon Monoxide in the Lower Troposphere. *J. Geophys. Res. Atmos.* **1998**, *103*, 19015–19033. [CrossRef]
6. Lu, Y.; Khalil, M.A.K. Methane and Carbon Monoxide in OH Chemistry: The Effects of Feedbacks and Reservoirs Generated by the Reactive Products. *Chemosphere* **1993**, *26*, 641–655. [CrossRef]
7. Arias, P.A.; Bellouin, N.; Coppola, E.; Jones, R.G.; Krinner, G.; Marotzke, J.; Naik, V.; Palmer, M.D.; Plattner, G.-K.; Rogelj, J.; et al. *Climate Change 2021: The Physical Science Basis. Contribution of Working Group I to the Sixth Assessment Report of the Intergovernmental Panel on Climate Change*; Masson-Delmotte, V., Zhai, P., Pirani, A., Connors, S.L., Péan, C., Berger, S., Caud, N., Chen, Y., Goldfarb, L., Gomis, M.I., et al., Eds.; Cambridge University Press: Cambridge, UK; New York, NY, USA, 2021; pp. 33–144.

8. Hu, H.; Landgraf, J.; Detmers, R.; Borsdorff, T.; Aan de Brugh, J.; Aben, I.; Butz, A.; Hasekamp, O. Toward Global Mapping of Methane With TROPOMI: First Results and Intersatellite Comparison to GOSAT. *Geophys. Res. Lett.* **2018**, *45*, 3682–3689. [\[CrossRef\]](#)
9. Lorente, A.; Borsdorff, T.; Butz, A.; Hasekamp, O.; aan de Brugh, J.; Schneider, A.; Wu, L.; Hase, F.; Kivi, R.; Wunch, D.; et al. Methane Retrieved from TROPOMI: Improvement of the Data Product and Validation of the First 2 Years of Measurements. *Atmos. Meas. Tech.* **2021**, *14*, 665–684. [\[CrossRef\]](#)
10. Callewaert, S.; Brioude, J.; Langerock, B.; Duflot, V.; Fonteyn, D.; Müller, J.-F.; Metzger, J.-M.; Hermans, C.; Kumps, N.; Ramonet, M.; et al. Analysis of CO<sub>2</sub>, CH<sub>4</sub>, and CO Surface and Column Concentrations Observed at Réunion Island by Assessing WRF-Chem Simulations. *Atmos. Chem. Phys.* **2022**, *22*, 7763–7792. [\[CrossRef\]](#)
11. Richardson, S.J.; Miles, N.L.; Davis, K.J.; Lauvaux, T.; Martins, D.K.; Turnbull, J.C.; McKain, K.; Sweeney, C.; Cambaliza, M.O.L. Tower Measurement Network of In-Situ CO<sub>2</sub>, CH<sub>4</sub>, and CO in Support of the Indianapolis FLUX (INFLUX) Experiment. *Elem. Sci. Anthr.* **2017**, *5*, 59. [\[CrossRef\]](#)
12. Resovsky, A.; Ramonet, M.; Rivier, L.; Tarniewicz, J.; Ciais, P.; Steinbacher, M.; Mammarella, I.; Mölder, M.; Heliasz, M.; Kubistin, D.; et al. An Algorithm to Detect Non-Background Signals in Greenhouse Gas Time Series from European Tall Tower and Mountain Stations. *Atmos. Meas. Tech.* **2021**, *14*, 6119–6135. [\[CrossRef\]](#)
13. Pitt, J.R.; Allen, G.; Bauguitte, S.J.-B.; Gallagher, M.W.; Lee, J.D.; Drysdale, W.; Nelson, B.; Manning, A.J.; Palmer, P.I. Assessing London CO<sub>2</sub>, CH<sub>4</sub> and CO Emissions Using Aircraft Measurements and Dispersion Modelling. *Atmos. Chem. Phys.* **2019**, *19*, 8931–8945. [\[CrossRef\]](#)
14. Li, S.; Kim, Y.; Kim, J.; Kenea, S.T.; Goo, T.-Y.; Labzovskii, L.D.; Byun, Y.-H. In Situ Aircraft Measurements of CO<sub>2</sub> and CH<sub>4</sub>: Mapping Spatio-Temporal Variations over Western Korea in High-Resolutions. *Remote Sens.* **2020**, *12*, 3093. [\[CrossRef\]](#)
15. Kuze, A.; Suto, H.; Nakajima, M.; Hamazaki, T. Thermal and near Infrared Sensor for Carbon Observation Fourier-Transform Spectrometer on the Greenhouse Gases Observing Satellite for Greenhouse Gases Monitoring. *Appl. Opt. AO* **2009**, *48*, 6716–6733. [\[CrossRef\]](#) [\[PubMed\]](#)
16. Butz, A.; Guerlet, S.; Hasekamp, O.; Schepers, D.; Galli, A.; Aben, I.; Frankenberg, C.; Hartmann, J.-M.; Tran, H.; Kuze, A.; et al. Toward Accurate CO<sub>2</sub> and CH<sub>4</sub> Observations from GOSAT. *Geophys. Res. Lett.* **2011**, *38*, L14812. [\[CrossRef\]](#)
17. Jacob, D.J.; Turner, A.J.; Maasakkers, J.D.; Sheng, J.; Sun, K.; Liu, X.; Chance, K.; Aben, I.; McKeever, J.; Frankenberg, C. Satellite Observations of Atmospheric Methane and Their Value for Quantifying Methane Emissions. *Atmos. Chem. Phys.* **2016**, *16*, 14371–14396. [\[CrossRef\]](#)
18. Butz, A.; Galli, A.; Hasekamp, O.; Landgraf, J.; Tol, P.; Aben, I. TROPOMI Aboard Sentinel-5 Precursor: Prospective Performance of CH<sub>4</sub> Retrievals for Aerosol and Cirrus Loaded Atmospheres. *Remote Sens. Environ.* **2012**, *120*, 267–276. [\[CrossRef\]](#)
19. Veefkind, J.P.; Aben, I.; McMullan, K.; Förster, H.; de Vries, J.; Otter, G.; Claas, J.; Eskes, H.J.; de Haan, J.F.; Kleipool, Q.; et al. TROPOMI on the ESA Sentinel-5 Precursor: A GMES Mission for Global Observations of the Atmospheric Composition for Climate, Air Quality and Ozone Layer Applications. *Remote Sens. Environ.* **2012**, *120*, 70–83. [\[CrossRef\]](#)
20. Sha, M.K.; De Mazière, M.; Notholt, J.; Blumenstock, T.; Chen, H.; Dehn, A.; Griffith, D.W.T.; Hase, F.; Heikkinen, P.; Hermans, C.; et al. Intercomparison of Low- and High-Resolution Infrared Spectrometers for Ground-Based Solar Remote Sensing Measurements of Total Column Concentrations of CO<sub>2</sub>, CH<sub>4</sub>, and CO. *Atmos. Meas. Tech.* **2020**, *13*, 4791–4839. [\[CrossRef\]](#)
21. Tu, Q. Observation of Atmospheric Greenhouse Gas Abundances on Regional Scales in Boreal Areas Using Portable FTIR Spectrometers. Ph.D. Thesis, Karlsruher Institut für Technologie (KIT), Karlsruhe, Germany, 2019.
22. Wunch, D.; Toon, G.C.; Blavier, J.-F.L.; Washenfelder, R.A.; Notholt, J.; Connor, B.J.; Griffith, D.W.T.; Sherlock, V.; Wennberg, P.O. The Total Carbon Column Observing Network. *Philos. Trans. R. Soc. A Math. Phys. Eng. Sci.* **2011**, *369*, 2087–2112. [\[CrossRef\]](#)
23. Frey, M.; Sha, M.K.; Hase, F.; Kiel, M.; Blumenstock, T.; Harig, R.; Surawicz, G.; Deutscher, N.M.; Shiomi, K.; Franklin, J.E.; et al. Building the COllaborative Carbon Column Observing Network (COCCON): Long-Term Stability and Ensemble Performance of the EM27/SUN Fourier Transform Spectrometer. *Atmos. Meas. Tech.* **2019**, *12*, 1513–1530. [\[CrossRef\]](#)
24. Herkommer, B.; Alberti, C.; Castracane, P.; Chen, J.; Dehn, A.; Dietrich, F.; Deutscher, N.M.; Frey, M.M.; Groß, J.; Gillespie, L.; et al. Using a Portable FTIR Spectrometer to Evaluate the Consistency of Total Carbon Column Observing Network (TCCON) Measurements on a Global Scale: The Collaborative Carbon Column Observing Network (COCCON) Travel Standard. *Atmos. Meas. Tech.* **2024**, *17*, 3467–3494. [\[CrossRef\]](#)
25. Gisi, M.; Hase, F.; Dohe, S.; Blumenstock, T.; Simon, A.; Keens, A. XCO<sub>2</sub>-Measurements with a Tabletop FTS Using Solar Absorption Spectroscopy. *Atmos. Meas. Tech.* **2012**, *5*, 2969–2980. [\[CrossRef\]](#)
26. Hase, F.; Frey, M.; Kiel, M.; Blumenstock, T.; Harig, R.; Keens, A.; Orphal, J. Addition of a Channel for XCO Observations to a Portable FTIR Spectrometer for Greenhouse Gas Measurements. *Atmos. Meas. Tech.* **2016**, *9*, 2303–2313. [\[CrossRef\]](#)
27. Jacobs, N.; Simpson, W.R.; Wunch, D.; O'Dell, C.W.; Osterman, G.B.; Hase, F.; Blumenstock, T.; Tu, Q.; Frey, M.; Dubey, M.K.; et al. Quality Controls, Bias, and Seasonality of CO<sub>2</sub> Columns in the Boreal Forest with Orbiting Carbon Observatory-2, Total Carbon Column Observing Network, and EM27/SUN Measurements. *Atmos. Meas. Tech.* **2020**, *13*, 5033–5063. [\[CrossRef\]](#)
28. Alberti, C.; Tu, Q.; Hase, F.; Makarova, M.V.; Gribanov, K.; Foka, S.C.; Zakharov, V.; Blumenstock, T.; Buchwitz, M.; Diekmann, C.; et al. Investigation of Spaceborne Trace Gas Products over St Petersburg and Yekaterinburg, Russia, by Using COllaborative Carbon Column Observing Network (COCCON) Observations. *Atmos. Meas. Tech.* **2022**, *15*, 2199–2229. [\[CrossRef\]](#)



29. Frey, M.M.; Hase, F.; Blumenstock, T.; Dubravica, D.; Groß, J.; Göttsche, F.; Handjaba, M.; Amadhila, P.; Mushi, R.; Morino, I.; et al. Long-Term Column-Averaged Greenhouse Gas Observations Using a COCCON Spectrometer at the High-Surface-Albedo Site in Gobabeb, Namibia. *Atmos. Meas. Tech.* **2021**, *14*, 5887–5911. [\[CrossRef\]](#)
30. Makarova, M.V.; Alberti, C.; Ionov, D.V.; Hase, F.; Foka, S.C.; Blumenstock, T.; Warneke, T.; Virolainen, Y.A.; Kostsov, V.S.; Frey, M.; et al. Emission Monitoring Mobile Experiment (EMME): An Overview and First Results of the St. Petersburg Megacity Campaign 2019. *Atmos. Meas. Tech.* **2021**, *14*, 1047–1073. [\[CrossRef\]](#)
31. Tu, Q.; Hase, F.; Schneider, M.; García, O.; Blumenstock, T.; Borsdorff, T.; Frey, M.; Khosrawi, F.; Lorente, A.; Alberti, C.; et al. Quantification of CH<sub>4</sub> Emissions from Waste Disposal Sites near the City of Madrid Using Ground- and Space-Based Observations of COCCON, TROPOMI and IASI. *Atmos. Chem. Phys.* **2022**, *22*, 295–317. [\[CrossRef\]](#)
32. Chen, J.; Viatte, C.; Hedelius, J.K.; Jones, T.; Franklin, J.E.; Parker, H.; Gottlieb, E.W.; Wennberg, P.O.; Dubey, M.K.; Wofsy, S.C. Differential Column Measurements Using Compact Solar-Tracking Spectrometers. *Atmos. Chem. Phys.* **2016**, *16*, 8479–8498. [\[CrossRef\]](#)
33. Hase, F.; Frey, M.; Blumenstock, T.; Groß, J.; Kiel, M.; Kohlhepp, R.; Mengistu Tsidu, G.; Schäfer, K.; Sha, M.K.; Orphal, J. Application of Portable FTIR Spectrometers for Detecting Greenhouse Gas Emissions of the Major City Berlin. *Atmos. Meas. Tech.* **2015**, *8*, 3059–3068. [\[CrossRef\]](#)
34. Klappenbach, F.; Bertleff, M.; Kostinek, J.; Hase, F.; Blumenstock, T.; Agustí-Panareda, A.; Razinger, M.; Butz, A. Accurate Mobile Remote Sensing of XCO<sub>2</sub> and XCH<sub>4</sub> Latitudinal Transects from Aboard a Research Vessel. *Atmos. Meas. Tech.* **2015**, *8*, 5023–5038. [\[CrossRef\]](#)
35. Luther, A.; Kleinschek, R.; Scheidweiler, L.; Defratyka, S.; Stanisavljevic, M.; Forstmaier, A.; Dandocsi, A.; Wolff, S.; Dubravica, D.; Wildmann, N.; et al. Quantifying CH<sub>4</sub> Emissions from Hard Coal Mines Using Mobile Sun-Viewing Fourier Transform Spectrometry. *Atmos. Meas. Tech.* **2019**, *12*, 5217–5230. [\[CrossRef\]](#)
36. Butz, A.; Hanft, V.; Kleinschek, R.; Frey, M.M.; Müller, A.; Knapp, M.; Morino, I.; Agustí-Panareda, A.; Hase, F.; Landgraf, J.; et al. Versatile and Targeted Validation of Space-Borne XCO<sub>2</sub>, XCH<sub>4</sub> and XCO Observations by Mobile Ground-Based Direct-Sun Spectrometers. *Front. Remote Sens.* **2022**, *2*, 775805. [\[CrossRef\]](#)
37. Agustí-Panareda, A.; Massart, S.; Chevallier, F.; Balsamo, G.; Boussetta, S.; Dutra, E.; Beljaars, A. A Biogenic CO<sub>2</sub> Flux Adjustment Scheme for the Mitigation of Large-Scale Biases in Global Atmospheric CO<sub>2</sub> Analyses and Forecasts. *Atmos. Chem. Phys.* **2016**, *16*, 10399–10418. [\[CrossRef\]](#)
38. Agustí-Panareda, A.; Massart, S.; Chevallier, F.; Boussetta, S.; Balsamo, G.; Beljaars, A.; Ciais, P.; Deutscher, N.M.; Engelen, R.; Jones, L.; et al. Forecasting Global Atmospheric CO<sub>2</sub>. *Atmos. Chem. Phys.* **2014**, *14*, 11959–11983. [\[CrossRef\]](#)
39. Alberti, C.; Hase, F.; Frey, M.; Dubravica, D.; Blumenstock, T.; Dehn, A.; Castracane, P.; Surawicz, G.; Harig, R.; Baier, B.C.; et al. Improved Calibration Procedures for the EM27/SUN Spectrometers of the Collaborative Carbon Column Observing Network (COCCON). *Atmos. Meas. Tech.* **2022**, *15*, 2433–2463. [\[CrossRef\]](#)
40. Frey, M.; Hase, F.; Blumenstock, T.; Groß, J.; Kiel, M.; Mengistu Tsidu, G.; Schäfer, K.; Sha, M.K.; Orphal, J. Calibration and Instrumental Line Shape Characterization of a Set of Portable FTIR Spectrometers for Detecting Greenhouse Gas Emissions. *Atmos. Meas. Tech.* **2015**, *8*, 3047–3057. [\[CrossRef\]](#)
41. Butz, A.; Dinger, A.S.; Bobrowski, N.; Kostinek, J.; Fieber, L.; Fischerkeller, C.; Giuffrida, G.B.; Hase, F.; Klappenbach, F.; Kuhn, J.; et al. Remote Sensing of Volcanic CO<sub>2</sub>, HF, HCl, SO<sub>2</sub>, and BrO in the Downwind Plume of Mt. Etna. *Atmos. Meas. Tech.* **2017**, *10*, 1–14. [\[CrossRef\]](#)
42. Tu, Q.; Hase, F.; Blumenstock, T.; Kivi, R.; Heikkinen, P.; Sha, M.K.; Raffalski, U.; Landgraf, J.; Lorente, A.; Borsdorff, T.; et al. Intercomparison of Atmospheric CO<sub>2</sub> and CH<sub>4</sub> Abundances on Regional Scales in Boreal Areas Using Copernicus Atmosphere Monitoring Service (CAMS) Analysis, Collaborative Carbon Column Observing Network (COCCON) Spectrometers, and Sentinel-5 Precursor Satellite Observations. *Atmos. Meas. Tech.* **2020**, *13*, 4751–4771. [\[CrossRef\]](#)
43. Tu, Q.; Hase, F.; Blumenstock, T.; Schneider, M.; Schneider, A.; Kivi, R.; Heikkinen, P.; Ertl, B.; Diekmann, C.; Khosrawi, F.; et al. Intercomparison of Arctic XH<sub>2</sub>O Observations from Three Ground-Based Fourier Transform Infrared Networks and Application for Satellite Validation. *Atmos. Meas. Tech.* **2021**, *14*, 1993–2011. [\[CrossRef\]](#)
44. Borsdorff, T.; aan de Brugh, J.; Schneider, A.; Lorente, A.; Birk, M.; Wagner, G.; Kivi, R.; Hase, F.; Feist, D.G.; Sussmann, R.; et al. Improving the TROPOMI CO Data Product: Update of the Spectroscopic Database and Destripping of Single Orbits. *Atmos. Meas. Tech.* **2019**, *12*, 5443–5455. [\[CrossRef\]](#)
45. Sha, M.K.; Langerock, B.; Blavier, J.-F.L.; Blumenstock, T.; Borsdorff, T.; Buschmann, M.; Dehn, A.; De Mazière, M.; Deutscher, N.M.; Feist, D.G.; et al. Validation of Methane and Carbon Monoxide from Sentinel-5 Precursor Using TCCON and NDACC-IRWG Stations. *Atmos. Meas. Tech.* **2021**, *14*, 6249–6304. [\[CrossRef\]](#)
46. Agustí-Panareda, A.; Barré, J.; Massart, S.; Inness, A.; Aben, I.; Ades, M.; Baier, B.C.; Balsamo, G.; Borsdorff, T.; Bousserez, N.; et al. Technical Note: The CAMS Greenhouse Gas Reanalysis from 2003 to 2020. *Atmos. Chem. Phys.* **2023**, *23*, 3829–3859. [\[CrossRef\]](#)
47. Agustí-Panareda, A.; Diamantakis, M.; Bayona, V.; Klappenbach, F.; Butz, A. Improving the Inter-Hemispheric Gradient of Total Column Atmospheric CO<sub>2</sub> and CH<sub>4</sub> in Simulations with the ECMWF Semi-Lagrangian Atmospheric Global Model. *Geosci. Model Dev.* **2017**, *10*, 1–18. [\[CrossRef\]](#)
48. Agustí-Panareda, A.; Diamantakis, M.; Massart, S.; Chevallier, F.; Muñoz-Sabater, J.; Barré, J.; Curcoll, R.; Engelen, R.; Langerock, B.; Law, R.M.; et al. Modelling CO<sub>2</sub> Weather—Why Horizontal Resolution Matters. *Atmos. Chem. Phys.* **2019**, *19*, 7347–7376. [\[CrossRef\]](#)

49. Koffi, N.; Bergamaschi, P. *Evaluation of Copernicus Atmosphere Monitoring Service Methane Products*; Publications Office of the European Union: Luxembourg, 2018. [[CrossRef](#)]
50. Tu, Q.; Hase, F.; Qin, K.; Cohen, J.B.; Khosrawi, F.; Zou, X.; Schneider, M.; Lu, F. Quantifying CH<sub>4</sub> Emissions from Coal Mine Aggregation Areas in Shanxi, China, Using TROPOMI Observations and the Wind-Assigned Anomaly Method. *Atmos. Chem. Phys.* **2024**, *24*, 4875–4894. [[CrossRef](#)]
51. Fiehn, A.; Kostinek, J.; Eckl, M.; Klausner, T.; Gałkowski, M.; Chen, J.; Gerbig, C.; Röckmann, T.; Maazallahi, H.; Schmidt, M.; et al. Estimating CH<sub>4</sub>, CO<sub>2</sub> and CO Emissions from Coal Mining and Industrial Activities in the Upper Silesian Coal Basin Using an Aircraft-Based Mass Balance Approach. *Atmos. Chem. Phys.* **2020**, *20*, 12675–12695. [[CrossRef](#)]
52. Trenchev, P.; Dimitrova, M.; Avetisyan, D. Huge CH<sub>4</sub>, NO<sub>2</sub> and CO Emissions from Coal Mines in the Kuznetsk Basin (Russia) Detected by Sentinel-5P. *Remote Sens.* **2023**, *15*, 1590. [[CrossRef](#)]
53. Li, J.; Li, X.; Chen, S.; Cao, J.; Gao, F. Study on Generation, Migration and Accumulation of CO in the Mining Goaf of Shallow-Buried Close Distance Coal Seam Group. *Sci. Rep.* **2022**, *12*, 14424. [[CrossRef](#)]

**Disclaimer/Publisher’s Note:** The statements, opinions and data contained in all publications are solely those of the individual author(s) and contributor(s) and not of MDPI and/or the editor(s). MDPI and/or the editor(s) disclaim responsibility for any injury to people or property resulting from any ideas, methods, instructions or products referred to in the content.